Rheology of Foams and Highly Concentrated Emulsions

I. Elastic Properties and Yield Stress of a Cylindrical Model System

H. M. PRINCEN

Exxon Research and Engineering Company, Corporate Research Laboratory, Linden, New Jersey 07036

Received February 22, 1982; accepted May 14, 1982

Expressions are derived for certain rheological properties, such as the stress vs strain relationship, yield stress, and shear modulus, of monodisperse foams and highly concentrated emulsions for the model of infinitely long cylindrical drops (or bubbles). The variables considered are the volume fraction of the dispersed phase, the drop radius, the interfacial tension, the thickness of the films separating adjacent drops, and the films' associated contact angle. Both the yield stress and the shear modulus are proportional to the interfacial tension and inversely proportional to the drop radius. The yield stress increases sharply with increasing volume fraction, while the shear modulus varies as its square root. The effect of a finite contact angle, θ, is to decrease the shear modulus and, in most cases, to increase the yield stress. Finally, the effect of a finite film thickness is to always increase both the yield stress and the shear modulus. The implications of these results to real emulsions and foams are discussed.

INTRODUCTION

Foams and highly concentrated emulsions are of importance in a multitude of practical applications. Much of their utility derives from their peculiar rheological properties, such as the high viscosity, relative to that of the constituent bulk fluid phases, a yield stress, and their shear-thinning behavior. What little experimental work exists suggests the following trends:

(1) Both the yield stress and the apparent viscosity increase with increasing volume fraction of the dispersed phase (1–3), and with decreasing bubble (or drop) size (1).

(2) Yield stresses of typical emulsions with volume fractions of the dispersed phase in excess of 0.90 are of the order of a few hundred to a few thousand dynes/cm^2 (2–4), and much smaller for foams (1), presumably as a result of the generally much larger size of the dispersed units.

(3) The observed flow behavior depends strongly on the nature of the contacting solid surfaces (4).

(4) Both emulsions and foams can be destroyed when subjected to sufficiently high shear (3, 4).

While experimental work on the rheology of these systems is scant, there appears to be a virtual lack of theoretical understanding of how the rheological properties are linked in a quantitative way to system parameters such as volume fraction of the dispersed phase, droplet (or bubble) size, interfacial tension, interfacial viscosity, contact angle between droplets (5–8), and thickness of the film separating adjacent drops (or bubbles).

It is the object of the present study to further this understanding by a detailed analysis of the deformation of the individual dispersed units when the system as a whole is subjected to strain, and by an analysis of the associated stress. In this first part, we shall concentrate on a two-dimensional model sys-

0021-9797/83/010160-16$03.00/0

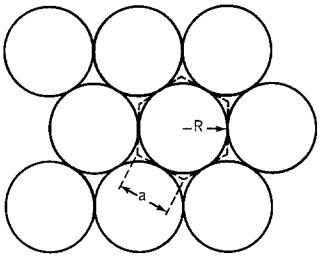

FIG. 1. Hexagonally close-packed cylindrical drops of radius R. Each drop is "contained" in a hexagon of side a. The volume fraction in this case is $\phi = 0.9069$.

tem, in which the dispersed units are cylindrical. Although such a system is unrealistic, it can be treated with relative ease and establishes the principles by which real foams and emulsions are governed. It may also facilitate subsequent analysis of the real, three-dimensional system. This step-wise approach was used successfully in a previous study of the structure of unstrained, highly concentrated emulsions (5, 6).

In the following, we shall refer to the system as an "emulsion" and to the dispersed units as "drops," although the analysis is equally valid for foams.

THEORETICAL ANALYSIS

Princen (5) presented an analysis of the geometrical packing and shape of cylindrical drops in a monodisperse, two-dimensional emulsion system when the volume fraction exceeds that of the system of hexagonally close-packed circular cylinders ($\phi = 0.9069$). The variables considered were the volume fraction, ϕ; the contact angle, θ, associated with the thin liquid films separating adjacent droplets (5–8); and the thickness, h, of these films. Other variables, i.e., the droplet radius, R, and the interfacial tension, γ, were shown to be involved in determining important emulsion properties, such as the compressive pressure exerted on the films (which must be balanced by a repulsive or "disjoining" pressure inside the films) and the emulsion's "osmotic pressure" (5, 6).

The results of the above study serve as a starting point for the present analysis. As before we shall first consider the case where the contact angle, θ, is zero, and the film thickness, h, is negligible compared to the overall drop dimensions. These restrictions will be relaxed later.

1. Zero Contact Angle; Negligible Film Thickness

As the volume fraction of a monodisperse, two-dimensional emulsion is increased, a point is reached where the drops, each of radius R, just touch and arrange themselves in a hexagonally close-packed configuration (Fig. 1). This occurs at $\phi = 0.9069$. At higher volume fractions, each drop occupies an increasingly large fraction of the hexagon (of side length a), available to it. In the process, the drop flattens at its six sides, where it is now separated from its neighbors by a thin flat film of continuous phase, while its surfaces in the corners are circular of radius r. This process continues until, at $\phi \rightarrow 1$, the drop has, in fact, assumed the shape of a pure hexagon (Fig. 2).

From Princen (5), we know that R, r, and ϕ are related through

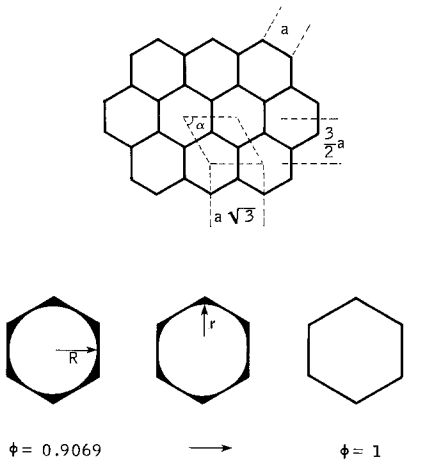

FIG. 2. Hexagonally close-packed cylindrical drops. The bottom sequence shows increased filling of the circumscribing hexagon as the volume fraction is raised. The dashed parallelogram is the unit cell used in the analysis.

$$R/a = \left(\frac{3\sqrt{3}}{2\pi}\right)^{1/2} \phi^{1/2} = 0.9094\phi^{1/2} \quad [1]$$

$$r/a = \left(\frac{3\sqrt{3}/2}{2\sqrt{3} - \pi}\right)^{1/2} (1 - \phi)^{1/2}$$

$$= 2.8383(1 - \phi)^{1/2} \quad [2]$$

and

$$R/r = \left(\frac{2\sqrt{3} - \pi}{\pi}\right)^{1/2} \frac{\phi^{1/2}}{(1 - \phi)^{1/2}}$$

$$= 0.3204 \frac{\phi^{1/2}}{(1 - \phi)^{1/2}}. \quad [3]$$

Let us consider such an emulsion to be contained between two horizontal, parallel plates in such a way that the outer drop layers are in intimate contact with the plates. The individual droplets in these outer layers will be flattened against the plates, and we shall assume that there is no "slip" at the droplet/plate interface. When the plates are forced to move relative to one another over a finite distance, the emulsion will be strained uniformly throughout its mass. Each layer of droplets, running parallel to the plates, will be displaced relative to the two adjacent layer. Because of droplet crowding, this can be accomplished only if each droplet is deformed in the process. To analyze this situation of simple shear, we shall consider what happens in cross section to a "unit cell," i.e., the parallelogram that connects the centers of four neighboring drops, as illustrated in Fig. 2. The base of this unit cell is $a\sqrt{3}$, and its height is $3a/2$. When strain is applied, the upper side of the unit cell moves relative to the base over a distance Δx, while the height and base are held constant. In this process, the angle α in the upper left-hand corner of the unit cell increases from an initial value of 60°, such that

$$\Delta x/a = \frac{3}{2}\cot 60° - \frac{3}{2}\cot \alpha$$

$$= \sqrt{3}/2 - \frac{3}{2}\cot \alpha. \quad [4]$$

The "strain," as commonly defined, equals the relative displacement of two shear planes divided by the distance between these planes, i.e.,

$$\text{Strain} = \frac{\Delta x}{3a/2} = \frac{2}{3}\Delta x/a$$

$$= 1/\sqrt{3} - \cot \alpha. \quad [4']$$

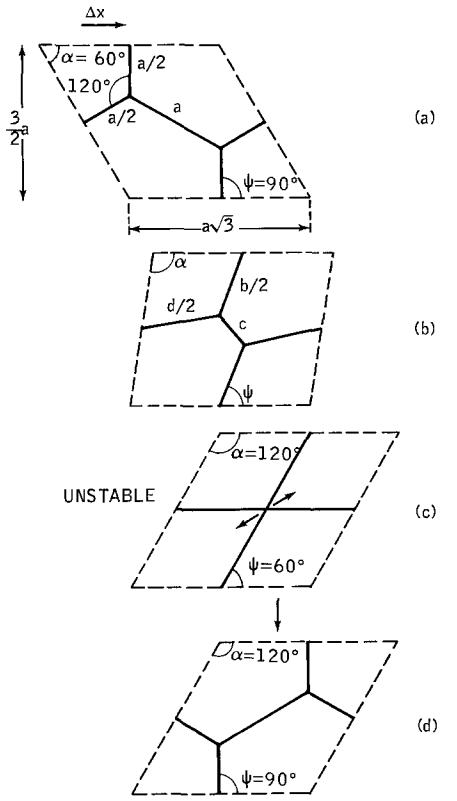

FIG. 3. Increasingly strained unit cell for $\phi = 1$. When $\alpha = 120°$ (or $\Delta x = a\sqrt{3}$), an instability arises and the original configuration is restored. (a) Unstrained; (b) strained, but below stability limit; (c) strained to stability limit; and (d) unstrained, after droplet reorientation.

It is assumed throughout that the films separating the droplets are stabilized against rupture by a suitable surfactant, so that drop coalescence does not occur.

i. Analysis for $\phi = 1$. The easiest case to treat is that for the limiting case of $\phi = 1$. The corresponding unstrained unit cell is shown in Fig. 3a. Anticipating our results, we conclude that, with increasing strain, the lengths of the films emanating from the centers of the sides of the unit cell increase from

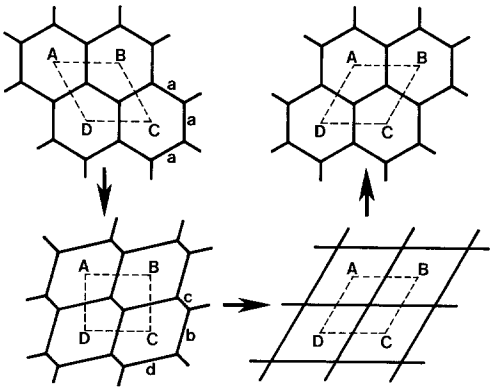

FIG. 4. Similar to Fig. 3 but with the four drops surrounding a given unit cell drawn in their entirety.

the initial values of $a/2$ to $b/2$ and $d/2$, respectively, while the "diagonally" oriented film decreases in length from a to c (Fig. 3b). In the process, the *total* surface area increases. At any stage, the films must meet at angles of 120° to ensure mechanical stability at the junctures (9–12). This condition is known as Lamarle's first law (12), formulated over a century ago (13, 14), and is consistent with that of minimum total surface area of the films within a given unit cell. It turns out that, at $\alpha = 120°$ and $\Delta x/a = \sqrt{3}$, the two intersection points merge into a single point (Fig. 3c). This configuration is unstable, as no more than three liquid films can meet in a line (9–12). The instability resolves itself by the generation of new film from the center to restore the original, unstrained configuration of lower total film area (Fig. 3d). The upper drop layer has now moved to the right by one drop width, relative to the stationary bottom layer. From then on, the process can repeat itself over and over again.

Instabilities of the type shown in Figs. 3c and d have been observed by Schwarz (11) in foams. He observed rearrangements within the foam as a result of the diffusion of gas from the smaller into the larger bubbles. Whenever a configuration such as that in Fig. 3c would develop as a consequence of, say, the disappearance of a particular film, the juncture of the four intersecting films would instantaneously disproportionate into two junctures by the generation of a new film until all films would again meet at angles of 120°.

The unit cell, as defined above, was chosen to facilitate the geometric analysis of the problem, perhaps at the expense of easy visualization of what happens to each individual drop. This can be readily remedied by fitting together a few unit cells, as shown in Fig. 4 where the four drops, whose centers are at the corners of the unit cell ABCD, have been drawn in their entirety at various stages in the straining cycle. From Fig. 4 it is seen, more clearly than from Fig. 3, that, although the emulsion as a whole is subjected to simple shear deformation, the drops respond in a more complex manner which is dictated by the requirement that the angles between intersecting films are to be maintained at 120°.

To proceed with the analysis, it is necessary to establish the lengths of the films, b, c, and d, at any stage in the above process. Also, the value of ψ, i.e., the angle between film b and the horizontal, needs to be evaluated, since this will give us the contribution to the stress per unit cell through

$$F = 2\gamma \cos \psi. \qquad [5]$$

Equation [5] results from the realization that each film has a tension 2γ and that it is the *horizontal* component of this tension that contributes to the tangential stress on the plates that are used to strain the system.

Finally, since the width of the unit cell is $a\sqrt{3}$, there are $1/a\sqrt{3}$ unit cells per cm^2 in any horizontal plane, so that the stress on the plates, i.e., the force per cm^2, is given by:

$$\tau = \frac{F}{a\sqrt{3}} = \frac{2\gamma}{a\sqrt{3}} \tilde{F} \qquad [6]$$

where $\tilde{F} = F/2\gamma = \cos \psi$, or, in view of Eq. [1],

$$\tau = 1.050 \frac{\gamma}{R} \phi^{1/2} \tilde{F} \qquad [7]$$

which is valid for any volume fraction exceeding 0.9069, not just for $\phi = 1$.

To evaluate b, c, d and ψ as a function of Δx (or α), we consider the unit cell at some intermediate state of strain, i.e., for $60° < \alpha < 120°$ (Fig. 5). MP, NP, and OP are given by $d/2$, $b/2$, and $c/2$, respectively, while all angles around P are 120°.

The area of the unit cell is given by:

$$A = \frac{3\sqrt{3}}{2} a^2 = 8 \times \text{Area } \Delta\text{MNO}. \quad [8]$$

It is readily shown that

$$\text{Area } \Delta\text{MNO} = \frac{\sqrt{3}}{16}(bc + cd + bd) \quad [9]$$

so that, by combining Eqs. [8] and [9], we find:

$$BC + CD + BD = 3 \quad [10]$$

where $B = b/a$, $C = c/a$, and $D = d/a$.

Furthermore, the cosine rule applied to ΔMOP yields

$$\text{MO} = [(d/2)^2 + (c/2)^2 + cd/4]^{1/2} \quad [11]$$

while, at the same time,

$$\text{MO} = a\sqrt{3}/2. \quad [12]$$

Combination of Eqs. [11] and [12] gives

$$C^2 + D^2 + CD = 3. \quad [13]$$

Similarly,

$$\text{NO} = [(b/2)^2 + (c/2)^2 + bc/4]^{1/2} \quad [14]$$

and

$$\text{NO} = \frac{3a}{4 \sin \alpha} \quad [15]$$

so that

$$B^2 + C^2 + BC = \frac{9}{4 \sin^2 \alpha} \quad [16]$$

or

$$\alpha = \arcsin\left[\frac{3}{2}(B^2 + C^2 + BC)^{-1/2}\right]. \quad [17]$$

Finally,

$$\psi = 180° - \alpha - \varphi \quad [18]$$

or

$$\cos \psi = -\cos(\alpha + \varphi). \quad [19]$$

The sine rule, applied to ΔNPO, leads to

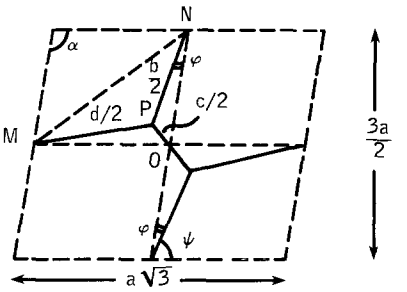

FIG. 5. Detailed view of unit cell for $\phi = 1$ at some intermediate state of strain.

$$\frac{\sin \varphi}{c/2} = \frac{\sin 120°}{\text{NO}}$$

or, because of Eq. [15],

$$\sin \varphi = C \sin \alpha/\sqrt{3}. \quad [20]$$

This, when combined with Eq. [19], yields

$$\cos \psi = \tilde{F} = -\cos\left(\alpha + \sin^{-1}\frac{C \sin \alpha}{\sqrt{3}}\right). \quad [21]$$

The solution to the problem can now proceed as follows. A value of C is picked between its limits of 1 and 0. The corresponding value of D is obtained from Eq. [13], and the corresponding value of B can then, in turn, be calculated from Eq. [10]. This enables one to evaluate α via Eq. [17]. Finally, $\tilde{F} = \cos \psi$ and the relative displacement of two adjacent layers, $\Delta x/a$, are obtained from Eqs. [21] and [4], respectively. This scheme is then repeated for different values of C, until the dependence of $\tilde{F}$ on displacement $\Delta x/a$ has been fully established.

The result is shown as the top curve in Fig. 6. The stress per unit cell, divided by twice the interfacial tension, increases up to a maximum value of $\tilde{F} = 0.5$ at $\Delta x/a = \sqrt{3}$, which is the situation depicted in Fig. 3c. At that point the stress drops abruptly to zero as the original geometry is restored. Thus, the emulsion behaves as a purely elastic material up to the yield stress, τ_0, which, on account of Eq. [7], is given by:

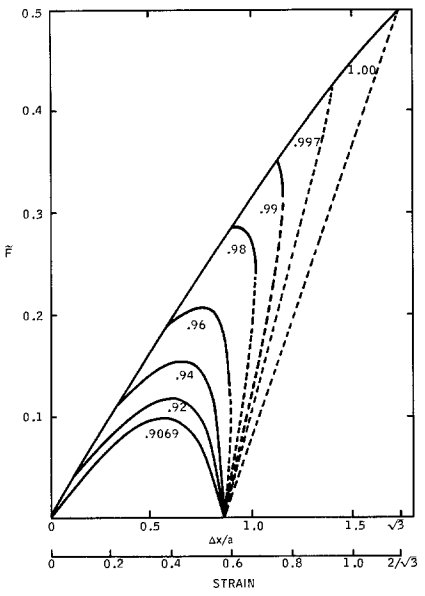

FIG. 6. Plot of $\tilde{F}$ vs $\Delta x/a$ for various values of ϕ. The top curve refers to $\phi = 1$. For lower values of ϕ, this same curve is followed over some range of $\Delta x/a$, until a so-called Mode-II configuration is reached and a different curve is followed which is physically meaningful only up to the point where it starts to back up.

$$\tau_0 = \frac{1.050}{2}\frac{\gamma}{R} = 0.525\gamma/R \quad (\phi = 1). \quad [22]$$

As an example, the yield stress of such a two-dimensional emulsion with $\gamma = 5$ dyn/cm and $R = 5$ μm would be $\tau_0 = 5250$ dyn/cm^2. Of course, when the applied stress exceeds τ_0, the emulsion will start, and continue, to flow.

ii. Analysis for 0.9069 ≤ φ < 1. For this case, the unstrained unit cell is shown in Fig. 7a. In this cross-section, the films no longer intersect in a point but meet in a triangular Plateau border whose sides have a radius of curvature, r, given by Eq. [2]. The angle enclosed by each pair of films is still 120°. It is clear that, initially at least, the process of straining the unit cell is identical to that described above for $\phi = 1$. The two Plateau borders maintain their shape and curvature as they are simply swept along with what used to be the two intersection points (Fig. 3). Therefore, over this so-called Mode-I range, $\tilde{F}$ will depend on $\Delta x/a$ in exactly the same manner as before. However, at some point, the two Plateau borders will come into "contact" (Fig. 7b), beyond which the two borders merge into one (Fig. 7c), giving rise to what we shall refer to as Mode-II configurations. The transition will occur the sooner, the larger the Plateau borders, i.e., the lower the volume fraction ϕ. The single channel, as shown in Fig. 7c, must have the same volume (i.e., the same cross-sectional area) as the two merging triangular Plateau borders, and its four bounding surfaces must have identical radii of curvature $\rho(\neq r)$, which will

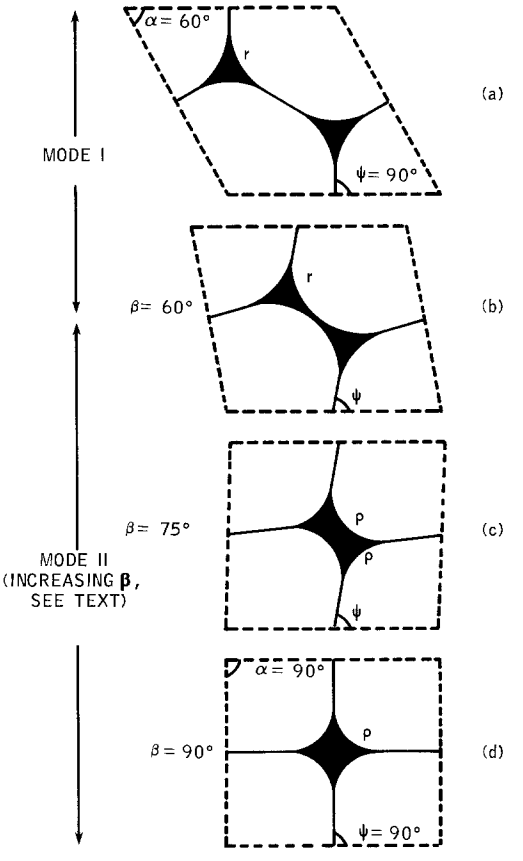

FIG. 7. Increasingly strained unit cell for $0.9069 < \phi < 1$ (a to c). The drawings are actual configurations for $\phi = 0.96$. Angle β is defined in Fig. 8 and is used as the independent variable in the analysis of the Mode-II region; (d) refers to $\alpha = \beta = 90°$ and is an unstable configuration, at least for $\phi > 0.96$.

now vary with the strain. In this situation, the films can no longer enclose angles of 120°.

The transition from Mode I to Mode II occurs at a value of $\Delta x/a$ where the length of c in Fig. 3 has decreased to just twice the center-to-cusp distance of each Plateau border, i.e.,

$$c_{tr} = 2r/\sqrt{3} \qquad [23]$$

where c_{tr} is the value of c at the transition, or, in view of Eq. [2],

$$C_{tr} = 3.2774(1 - \phi)^{1/2}. \qquad [24]$$

The corresponding values of D, B, α, $\Delta x/a$, and $\tilde{F}$ can be obtained, as before, from Eqs. [13], [10], [17], [4], and [21], respectively.

Beyond the transition, the previous analysis no longer applies. Instead, we refer to Fig. 8 for a detailed view of the unit cell at some point in this range. The lengths of the two remaining types of film are f_1 and f_2. As mentioned above, the radii of curvature of the bounding surfaces of the central channel are ρ. As an analytical aid, a diamond is constructed whose sides pass through the cusps of the channel, perpendicular to the films, so that its sides are 2ρ. It is further characterized by the angle β in its upper left-hand corner. At the Mode I → Mode II transition, $\beta = 60°$; it varies with the strain. The angles α_1 and α_2 are defined as in Fig. 8 ($\alpha_1 + \alpha_2 = \alpha$).

The cross-sectional area of the central channel is given by:

$$A_{ch} = 4\rho^2 \sin\beta - \pi\rho^2 \qquad [25]$$

so that the volume fraction is

$$\phi = \frac{A - A_{ch}}{A}$$

$$= 1 - \frac{2}{3\sqrt{3}}(\rho/a)^2(4\sin\beta - \pi) \qquad [26]$$

or

$$\rho/a = \left(\frac{3\sqrt{3}}{8\sin\beta - 2\pi}\right)^{1/2}(1 - \phi)^{1/2}. \qquad [27]$$

Straightforward but somewhat tedious geometric analysis, which will not be presented here, yields the following equations.[1] They have been arranged in such an order that each quantity can be evaluated from those listed above it. This facilitates sequential numerical computations.

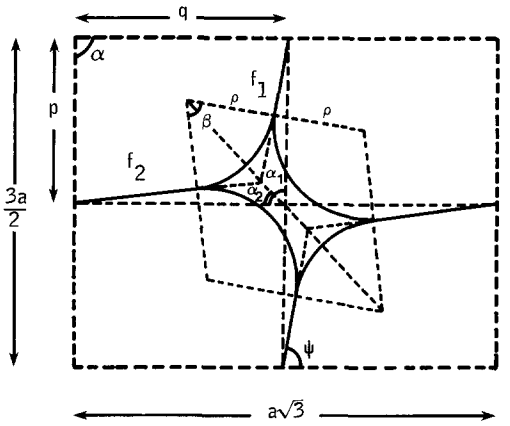

FIG. 8. Detailed view of unit cell for $\phi < 1$ when the configuration is of the Mode-II type (schematic).

$$q/\rho = \frac{\sqrt{3}/2}{\rho/a} \qquad [28]$$

$$f_2/\rho = -\sin\beta + [(q/\rho)^2 - \cos^2\beta]^{1/2} \qquad [29]$$

$$f_1/\rho = \frac{(\sqrt{3}/2)(q/\rho)^2 - \sin\beta - f_2/\rho}{(f_2/\rho)\sin\beta + 1} \qquad [30]$$

$$p/\rho = [(f_1/\rho)^2 + 2(f_1/\rho)\sin\beta + 1]^{1/2} \qquad [31]$$

$$\alpha_1 = \cos^{-1}\left(\frac{\cos\beta}{p/\rho}\right) - \beta/2 \qquad [32]$$

$$\alpha_2 = \cos^{-1}\left(\frac{\cos\beta}{q/\rho}\right) - \beta/2 \qquad [33]$$

$$\alpha = \alpha_1 + \alpha_2 \qquad [34]$$

$$\tilde{F} = \cos\psi = \sin(\alpha_2 - \beta/2) \qquad [35]$$

and, of course,

$$\Delta x/a = \sqrt{3}/2 - \frac{3}{2}\cot\alpha. \qquad [36]$$

The solution to the Mode-II part of the

[1] A list of derivations of these and other equations in this paper may be obtained from the author upon request.

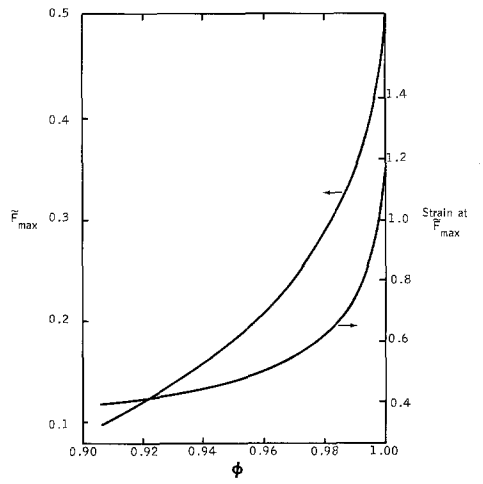

FIG. 9. $\tilde{F}_{max}$ and the corresponding strain as a function of ϕ.

problem proceeds as follows. Choose the volume fraction of interest in the range $0.9069 \leqslant \phi < 1$, and a value of β in the range $60° \leqslant \beta \leqslant 90°$. Working sequentially through Eqs. [27]–[36], one finally arrives at the corresponding values of $\tilde{F}$ and $\Delta x/a$. Then this scheme is repeated for a larger value of β until $\tilde{F}$ vs $\Delta x/a$ has been evaluated completely for that particular value of ϕ, etc.

The results for various values of ϕ are presented in Fig. 6, together with the previous curve for $\phi = 1$. The dashed parts of the curves, although representing mathematical solutions to the problem, are physically meaningless and refer to unstable states, much like the instabilities encountered when a solid object is pulled vertically out of a liquid. In the latter case, the force passes through a maximum with increasing vertical displacement (the "maximum force"), then decreases until the slope of the force vs displacement curve becomes infinite (the "maximum height") where the object detaches from the liquid surface. A typical theoretical force vs displacement curve backs up at this point but is not experimentally accessible in that region because it represents unstable equilibria [e.g., see Refs. (15–19)]. It will be shown later how this type of instability is handled in the present problem.

It is seen in Fig. 6 that for any ϕ, except for $\phi = 0.9069$, the curve initially follows that for $\phi = 1$ (Mode-I deformation). However, at the point of transition from Mode I to Mode II, the curve bends away and ultimately goes to zero at $\Delta x/a = \sqrt{3}/2$, where $\alpha = \beta = 90°$. For the lower volume fractions, the Mode-II curves pass through a maximum $\tilde{F}_{max}$. At higher ϕ, the maximum force is reached while the system is still in Mode I. $\tilde{F}_{max}$ is the unit cell's contribution to the yield stress of the system. The yield stress itself is given by Eq. [7] where $\tilde{F} = \tilde{F}_{max}$. Since, in the range of interest, ϕ varies only from 0.9069 to 1, the yield stress is, to a good approximation, given by:

$$\tau_0 \approx \frac{\gamma}{R} \cdot \tilde{F}_{max} . \qquad [37]$$

$\tilde{F}_{max}$ and the corresponding strain have been plotted as a function of ϕ in Fig. 9. $\tilde{F}_{max}$ is seen to increase sharply from about 0.1 at $\phi = 0.9069$ to 0.5 at $\phi = 1$.

If one could, in fact, produce cylindrical systems of the type being considered here, at least two kinds of experiment can be imagined.

First, one can use a stress-controlling device and subject the system to a given *stress*, τ. As long as $\tau < \tau_0$, the system will simply respond with an elastic deformation, characterized by the corresponding $\Delta x/a$. When $\tau \geqslant \tau_0$, however, the emulsion cannot develop sufficient elastic stress to balance τ, and the emulsion will start, and continue, to flow as long as the applied stress is maintained.

Second, one can use a strain-controlling device, impose a given *strain* on the system, and measure the resulting stress. In this situation, one can, in principle, explore the stress–strain relationship over a whole cycle, i.e., for $0 \leqslant \Delta x/a \leqslant \sqrt{3}$.

Figure 6 is incomplete for this purpose. To find the complete stress–strain curve for increasing $\Delta x/a$, two facts must be taken into account: (i) as indicated above, the curves are physically meaningful only up to the point where their tangent is vertical, i.e., where the

curves in Fig. 6 start to back up (dashed lines). When Δx is increased beyond that point, the system jumps to a new configuration where $\tilde{F}$ actually changes sign (see below). The new configuration may be either of Mode I or Mode II; (ii) the point in Fig. 6 where $\tilde{F} = 0$ and $\Delta x/a = \sqrt{3}/2$ is the merging point for all Mode-II curves. As noted before, $\alpha = \beta = 90°$ at this point, which means that the drops are then lined up in vertical rows, with the unit cell appearing as in Fig. 7d. Although this configuration may or may not be stable for reasons given above, it can be reached equally well, from a mathematical point of view, from the side of negative stress (by reversing the direction of strain, starting from $\Delta x/a = \sqrt{3}$). Therefore, this point can be seen as a center of symmetry, and all curves in Fig. 6 have their symmetrically disposed counterparts for $\tilde{F} < 0$. The corresponding configurations of the unit cell are mirror images of those for $\tilde{F} > 0$.

Keeping the above two facts in mind, one arrives at the complete stress–strain curves shown in Fig. 10 for continuously increasing strain over a whole cycle. As long as $\tilde{F} > 0$, the system will return to its original position at (0; 0) when it is suddenly set free to move. When $\tilde{F} < 0$, however, the system is driven "forward" to the end of the cycle at (0; $\sqrt{3}$). This may be termed the "toggle switch effect."

2. *Finite Contact Angle; Negligible Film Thickness*

The existence of contact angles in emulsions has been well established, particularly in systems stabilized by anionic surfactants in the presence of added electrolyte (6–8). This phenomenon can lead to an increased packing density of the emulsion, as discussed in great detail for cylindrical systems by Princen (5), and in less detail for real emulsions by Princen *et al.* (6). It is important to note that for a given value of the contact angle, θ, there is a certain volume fraction, ϕ_0^θ (>0.9069), at which the drops can pack in hexagonal close-packing without being

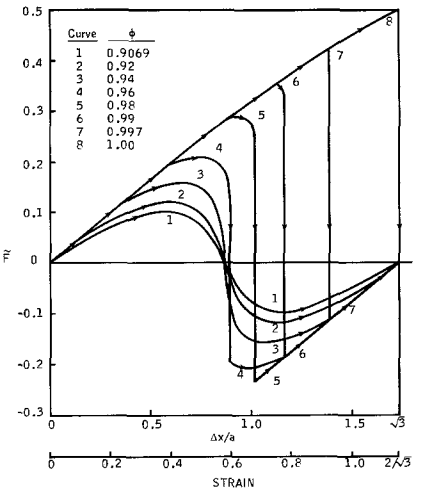

FIG. 10. Stress vs strain curves for different values of ϕ.

"compressed" (5). That is to say that a collection of drops, suspended freely in the continuous phase, has a tendency to *spontaneously* clump together to form a close-packed structure of volume fraction ϕ_0^θ, which is given by (see Ref. 5)

$$\phi_0^\theta = \frac{\pi - 6\theta + 3\sin 2\theta}{2\sqrt{3}\cos^2\theta} \quad (\theta \text{ in radians}) \qquad [38]$$

for $0 \leqslant \theta \leqslant 30°$. For $\theta \geqslant 30°$, $\phi_0^\theta = 1$.

The drops in such a structure are deformed, but not by the process of compression that is associated with trying to force more drops into a given volume of continuous phase than that corresponding to hexagonally close-packed, undeformable cylinders. Instead, the drops deform spontaneously, as they "make contact," under the influence of strong short-range attractive forces, the existence and magnitude of which are, in fact, indicated by the existence and magnitude of the contact angle.

It is not difficult to envisage an emulsion with $\phi > \phi_0^\theta$. This situation was discussed by Princen (5). The drops are then indeed compressed and will, no doubt, arrange themselves in a hexagonally close-packed structure. However, emulsions with $\phi < \phi_0^\theta$ are

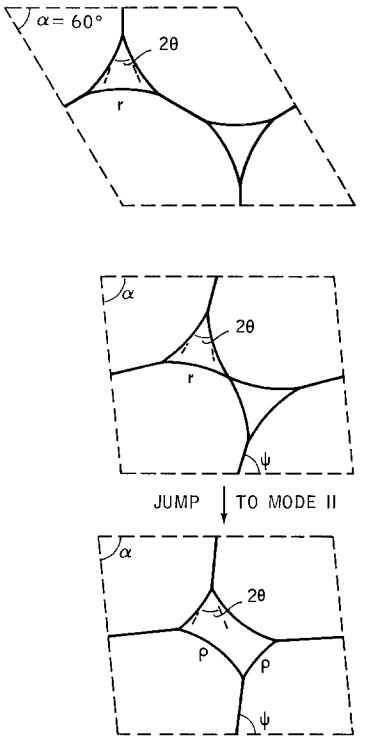

FIG. 11. Increasingly strained unit cell for $\theta > 0$ and $\phi > \phi_0^\theta$ (schematic).

more difficult to visualize. They contain more continuous phase than is consistent with their tendency to pack hexagonally to a volume fraction ϕ_0^θ. We speculate that the "excess" continuous phase is expelled from the structure, not necessarily as a bulk phase that can readily be separated from the remaining emulsion of $\phi = \phi_0^\theta$, but, more likely, as occluded pockets of continuous phase that are not spontaneously expelled from the overall emulsion. Working with real emulsions, we have observed such pockets [e.g., see Fig. 10B in Ref. (6)]. These could, at least partially, be removed by mild centrifugation. Upon subsequent relaxation, an emulsion layer was left of volume fraction close to, but always somewhat smaller than, ϕ_0^θ. The removal became more and more difficult as θ increased. As the occluded pockets of continuous phase confer a degree of disorder to the system, we shall initially restrict ourselves to systems with $\phi > \phi_0^\theta$.

The unit cell for such a system, at various stages in the straining process, is shown schematically in Fig. 11. Again, there is a region of Mode-I deformation, where the process is identical to that described above for $\phi = 1$, $\theta = 0$, except that the film tension is now reduced from 2γ to $2\gamma \cos\theta$ (7), so that at any stage the contribution, F, of the unit cell to the shear stress is now given by

$$F = 2\gamma \cos\theta \cos\psi$$

or, in dimensionless form,

$$\tilde{F} = F/2\gamma \cos\theta = \cos\psi. \qquad [39]$$

While Eq. [1] is still valid, Eqs. [2] and [3] now become (see Eqs. [27]–[28] of Ref. (5))

$$r/a = \frac{\sqrt{3}}{2\cos\theta}\left(\frac{1-\phi}{1-\phi_0^\theta}\right)^{1/2} \qquad [40]$$

and

$$R/r = \left(\frac{2\sqrt{3}}{\pi}\right)^{1/2} \times \cos\theta(1-\phi_0^\theta)^{1/2}\left(\frac{\phi}{1-\phi}\right)^{1/2} \qquad [41]$$

where ϕ_0^θ is given by Eq. [38].

The transition from Mode I to Mode II will again occur when the two Plateau borders meet, i.e., when c in Fig. 3 has decreased to just twice the center-to-cusp distance of each border; in this case

$$c_{tr} = \frac{4}{\sqrt{3}} r \sin(30° - \theta) \qquad [42]$$

or, in view of Eq. [40],

$$C_{tr} = \frac{2\sin(30° - \theta)}{\cos\theta}\left(\frac{1-\phi}{1-\phi_0^\theta}\right)^{1/2}. \qquad [43]$$

This, in the same manner as described above for $\theta = 0$, establishes the values of $\Delta x/a$ and of $\cos\psi = \tilde{F}$ on the Mode-I curve where the transition to Mode II occurs.

We have seen that, when $\theta = 0$, the transition is continuous. At the transition, ρ and r are synonymous and equal. When $\theta > 0$,

however, the transition is discontinuous; as soon as the Plateau borders "touch," a sudden rearrangement must take place toward the formation of a single central channel, whose radii of curvature, ρ, are different from r. This will be accompanied by a sudden change in ψ and, therefore, in $\tilde{F}$.

To analyze Mode II in detail, we again construct a diamond around the central channel, as in Fig. 12a. In this case, the cusps of the central channel are no longer located at the centers of the sides of this diamond.

The analysis is still straightforward but even more tedious than before. We list the relevant equations below, again without presenting their derivation.

$$\rho/a = \left(\frac{3\sqrt{3}}{8 \sin \beta \cos^2 \theta - 4 \sin 2\theta - 2\pi + 8\theta}\right)^{1/2} \times (1 - \phi)^{1/2} \quad [44]$$

where θ is expressed in radians,

$$q/\rho = \frac{\sqrt{3}/2}{\rho/a} \quad [45]$$

$$f_2/\rho = \sin \theta - \sin \beta \cos \theta + [(q/\rho)^2 - \cos^2 \theta \cos^2 \beta]^{1/2} \quad [46]$$

$$f_1/\rho = \frac{(\sqrt{3}/2)(q/\rho)^2 - \sin \beta + \sin 2\theta - (f_2/\rho)(\cos \theta - \sin \beta \sin \theta)}{(f_2/\rho) \sin \beta + \cos \theta - \sin \beta \sin \theta} \quad [47]$$

$$p/\rho = [(f_1/\rho)^2 + 2(f_1/\rho)(\sin \beta \cos \theta - \sin \theta) + 1 - \sin \beta \sin 2\theta]^{1/2} \quad [48]$$

$$\alpha_1 = \cos^{-1}\left(\frac{\cos \beta \cos \theta}{p/\rho}\right) - \beta/2 \quad [49]$$

$$\alpha_2 = \cos^{-1}\left(\frac{\cos \beta \cos \theta}{q/\rho}\right) - \beta/2 \quad [50]$$

$$\alpha = \alpha_1 + \alpha_2 \quad [51]$$

$$\Delta x/a = \sqrt{3}/2 - \frac{3}{2} \cot \alpha \quad [52]$$

and

$$\tilde{F} = F/2\gamma \cos \theta = \cos \psi = \sin (\alpha_2 - \beta/2). \quad [53]$$

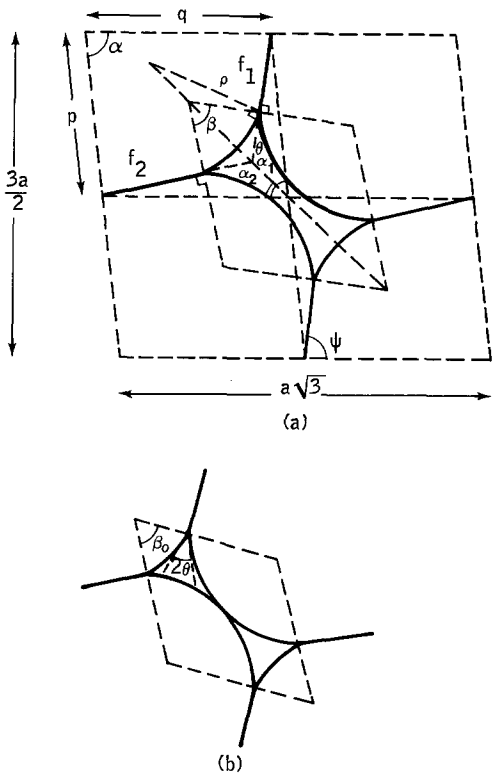

FIG. 12. (a) Detailed view of unit cell for a Mode-II configuration when $\theta > 0$ and $\phi > \phi_0^a$. (b) Limiting configuration, characterized by $\beta = \beta_0$, where a reduction in strain leads to a Mode II → Mode I jump.

It is readily verified that Eqs. [44]–[53] simplify to Eqs. [27]–[36] when $\theta = 0$.

As indicated before for $\theta = 0$, Eqs. [44]–[53] when evaluated in sequence, enable one to construct the $\tilde{F}$ vs $\Delta x/a$ curve for the Mode-II region for any combination of ϕ and θ by inserting increasing values of β between its appropriate limits. For $\theta = 0$, these limits were 60 and 90°. For $\theta > 0$, the upper limit is unchanged, but the lower limit is raised somewhat and corresponds to the case illustrated in Fig. 12b where the two long arcs just touch. (This configuration can be reached by reducing the strain from that in Fig. 12a.) It can be shown that this limiting Mode-II

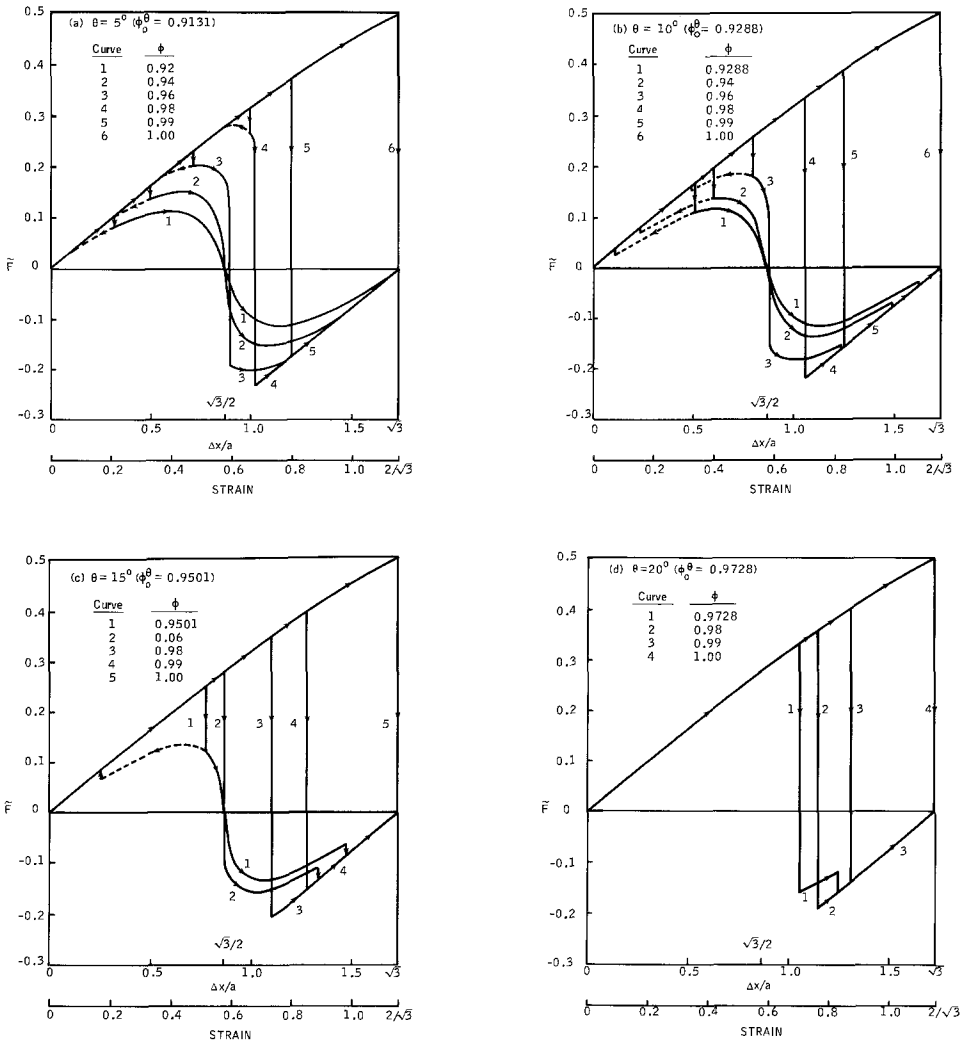

FIG. 13. Stress vs strain curves as a function of ϕ ($>\phi_0^\theta$) for several finite values of θ.

configuration occurs when $\beta = \beta_0$, where

$$\sin\frac{\beta_0}{2} = \frac{1}{2\cos\theta}. \qquad [54]$$

Lower values of β would imply interpenetration of the two long arcs in Fig. 12b, which is physically meaningless. Instead, the system jumps to a Mode-I configuration.

This Mode II → Mode I jump, coupled with the Mode I → Mode II jump noted above, can give rise to hysteresis loops in the complete stress–strain curves when the strain is reversed. Figure 13 shows some resulting curves for each of several values of θ. In the construction of these curves, the same factors were considered as in Fig. 10, i.e., the physical meaninglessness of those parts of the Mode-II curves that back up, and the symmetry about point (0; $\sqrt{3}/2$).

It is seen that, in all cases, the Mode-I curve is followed up to the point where the two Plateau borders touch. Then the stress suddenly drops, either to a smaller *positive* value, from where it continues on a Mode-II curve, or to a *negative* value. The latter occurs in those cases where the vertical

"jump line" does not intersect the corresponding Mode-II curve in the positive stress portion of the diagram. The jump may then end up on the symmetrically disposed Mode-II or Mode-I curve. When the strain is increased further, these curves are followed until, at point (0; $\sqrt{3}$) the original configuration is restored and adjacent layers have completed a relative translation of one unit cell. The process can then be repeated over and over.

The hysteresis loops, referred to above, are also indicated in Fig. 13. If, just following the Mode I → Mode II jump, the strain is reversed, the dashed Mode-II curve is followed until $\beta = \beta_0$ and the system reverts to a Mode-I configuration.

The yield stress, τ_0, is given by

$$\tau_0 = 1.050 \frac{\gamma \cos\theta}{R} \phi^{1/2} \tilde{F}_{max} \qquad [55]$$

where $\tilde{F}_{max}$ is the maximum positive value of $\tilde{F}$ in Fig. 13. In all but one of the illustrated cases, the maximum is reached while the system is in a Mode-I configuration. The only exception is the case of $\theta = 5°$ and $\phi = 0.9131$, where the absolute maximum is reached on the Mode-II curve, following the Mode I → Mode II jump.

The values of $\tilde{F}_{max}$ are plotted in Fig. 14 as a function of ϕ ($\geq \phi_0^\theta$) for several values of θ, including $\theta = 0$ (solid curves). It can be concluded that, in spite of the cos θ term in Eq. [55], the effect of a finite contact angle is to *increase* the yield stress, except in the region of very small θ and relatively small ϕ, and in the region of large θ and large ϕ, where the effect is reversed.

We speculated above that, when $\phi < \phi_0^\theta$, the emulsion contains pockets of occluded continuous phase, dispersed in a matrix emulsion of $\phi = \phi_0^\theta$. Provided these pockets are large compared to the emulsion droplets, it can be shown that the average number of films per unit area is reduced by a factor of ϕ/ϕ_0^θ vis-à-vis the emulsion of $\phi = \phi_0^\theta$. Thus, the stress in the stress–strain curve and, therefore, the yield stress are reduced, to a first approximation, by this same factor. This has been indicated in Fig. 14 by dashed lines for $\phi < \phi_0^\theta$.

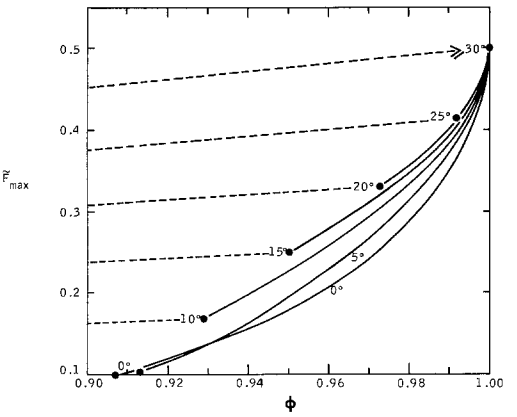

FIG. 14. $\tilde{F}_{max}$ as a function of ϕ and θ. Solid lines refer to $\phi > \phi_0^\theta$, dashed lines to $\phi < \phi_0^\theta$ and are speculative.

3. *Shear Modulus*

From the stress vs strain relationships discussed above, we derived quantitative expressions for the yield stress, τ_0. Another rheological parameter that is readily derived is the *shear modulus*, G', for small stresses (or strains), i.e., in the region prior to the yield stress, where the emulsion behaves as a purely elastic material.

G' is defined as

$$G' = \frac{\text{shear stress}}{\text{shear strain}}. \qquad [56]$$

The shear strain is given by 2/3 $\Delta x/a$ (see Eq. [4']), while the shear stress, τ, in its general form ($\theta \geq 0$), is given by the equivalent of Eq. [55]:

$$\tau = 1.050 \frac{\gamma \cos\theta}{R} \phi^{1/2} \tilde{F}. \qquad [57]$$

Substituting for stress and strain in Eq. [56], one finds

$$G' = 1.575 \frac{\gamma \cos\theta}{R} \phi^{1/2} \left(\frac{\tilde{F}}{\Delta x/a} \right). \qquad [58]$$

For all cases discussed above, except that for $\phi = 0.9069$ and $\theta = 0$, the curves of $\tilde{F}$ vs $\Delta x/a$ initially follow the Mode-I curve which, for small deformations, is essentially linear and of slope very close to 1/3, so that

$$G' = 0.525 \frac{\gamma \cos\theta}{R} \phi^{1/2} \quad \begin{pmatrix} \phi > 0.9069; \\ \text{small } \Delta x/a \end{pmatrix}. \qquad [59]$$

4. *Effect of Finite Film Thickness*

Up to this point, the thickness of the films separating individual droplets was considered to be negligible compared to the dimensions of each drop. When the drops are extremely small and the film thickness is relatively large (e.g., when the emulsion is stabilized by an ionic surfactant at low electrolyte concentration), this may not be a good approximation. It was shown for the unstrained system (cf. Eq. [17] in Ref. (5)) that, for finite film thickness, a given drop shape is found at a volume fraction, ϕ^h, that is somewhat smaller than the volume fraction, ϕ, at which that same drop shape would be found in a system with zero film thickness. The two volume fractions are related through

$$\frac{1}{\phi^h} = \left[\frac{1}{\phi^{1/2}} + \left(\frac{2\sqrt{3}}{\pi}\right)^{1/2} \frac{h}{2R}\right]^2 = \left[\frac{1}{\phi^{1/2}} + 1.050 \frac{h}{2R}\right]^2. \qquad [60]$$

It is readily shown that Eq. [60] is equally valid for the strained systems discussed in the present study. In other words, all phenomena described above for $h = 0$ remain valid with the proviso that the volume fractions are shifted downward in accordance with Eq. [60]. This implies that, for given volume fraction, the effect of a finite film thickness is to *increase* both the yield stress and shear modulus.

CONCLUSIONS AND DISCUSSION

For the two-dimensional model of a monodisperse, highly concentrated emulsion in simple shear, we have been able to derive the exact stress vs strain relationships in the elastic region as a function of the volume fraction, ϕ, and contact angle, θ. The effect of a finite film thickness, h, has also been indicated.

Exact predictions have been made of the yield stress, τ_0, and the shear modulus, G'. In the most general situation, the respective expressions are

$$\tau_0 = 1.050 \frac{\gamma \cos\theta}{R} \phi^{1/2} \tilde{F}_{max} \qquad [61]$$

where the last, dimensionless term depends on both ϕ and θ, and can be evaluated from Fig. 14, and

$$G' = 0.525 \frac{\gamma \cos\theta}{R} \phi^{1/2}. \qquad [62]$$

Both τ_0 and G' are directly proportional to the interfacial tension and inversely proportional to the drop radius. The dependence of G' on θ and ϕ is direct and simple; that of τ_0 is more complex because of the term $\tilde{F}_{max}$. The overall effect is that τ_0 increases sharply with increasing ϕ and, in most cases, increases also with increasing θ.

It will be extremely difficult to extend the analysis to *real* emulsions at the same level of detail. However, the same general relationships should apply. In fact, on the basis of simple analogy, we would expect the corresponding expressions for τ_0 and G' of real, monodisperse emulsions to read:

$$\tau_0 = C_1 \frac{\gamma \cos\theta}{R} \phi^{1/3} \tilde{F}_{max} \qquad [63]$$

and

$$G' = C_2 \frac{\gamma \cos\theta}{R} \phi^{1/3} \qquad [64]$$

where C_1 and C_2 are, as yet unknown, numerical constants, and $\tilde{F}_{max}$ depends in the same qualitative fashion on ϕ and θ as in the two-dimensional case, e.g., it will increase sharply with increasing ϕ. Of course, for real emulsions the range of ϕ that is of interest

is $0.74 \leqslant \phi \leqslant 1$, rather than $0.9069 \leqslant \phi \leqslant 1$. In preliminary experiments on a series of emulsions of different volume fractions but identical values of the interfacial tension and average droplet size, we have indeed observed such a sharp rise of the yield stress with increasing ϕ. Moreover, the measured yield stresses were of the same order of magnitude as those predicted by Eq. [61]. It will be interesting to test the simple dependence of τ_0 on γ and R when ϕ and R are kept constant. To our knowledge, this has not been done.

To fully understand the rheological behavior of real emulsions, it will be important to build polydispersity into the model. This we have not accomplished as yet, but we speculate that polydispersity will not invalidate Eqs. [61]–[64], provided that R is replaced by some average drop radius $\bar{R}$. Polydispersity is also expected to smear out some of the details in the stress–strain curves.

Another limitation of the current model is the assumption that the interfacial tension does not vary with strain. This may not always be strictly valid, since strain implies an increase in the surface area of each drop. For example, for $\phi \approx 1$, the increase in surface area at the end of a cycle can be shown to be about 15%. Even under static conditions of strain, this will in principle be accompanied by depletion of surfactant, and a consequent increase in interfacial tension. Particularly when the volume fraction is very high and the surfactant concentration is low, this can lead to destabilization of the liquid films separating the droplets. This mechanism of film destabilization and consequent drop coalescence becomes potentially even more severe when flow occurs, especially at high rates of shear, when diffusion of surfactant from the interior of the films and the Plateau borders into the surfaces of the expanding films may be too slow to maintain stability. This kind of destabilization of foams and high-internal-phase emulsions is well known in practice (3, 4, 20).

We are currently conducting an experimental study of the rheology of real high-internal-phase emulsions. To obtain meaningful and reproducible results, it appears essential that the viscometer walls are perfectly wetted by the continuous phase. Otherwise, the surface induces instability of the emulsion layer adjacent to the wall, which can lead to gross coalescence or formation of a thick, lubricating film of dispersed phase, as inferred by Mannheimer from his study of oil-in-water emulsions flowing through a Teflon tube (4). Even if the continuous phase *does* wet the viscometer walls, the interpretation of rheological measurements is complicated by the presence of a thin film of continuous phase between the outer layers of emulsion droplets and the solid walls. This film is expected to have a thickness that is comparable to that between the droplets, and gives rise to a degree of "slip." When properly interpreted, however, measurements may give information not only on the rheological properties of the emulsion itself, but on the effective thickness of the film as well. This will be a subject for future study.

Finally, the model described in this study is a static one. It does not treat the case of continuous flow, which is initiated when $\tau > \tau_0$. To extend the theory in this direction, i.e., to predict the dependence of shear stress on *shear rate*, a detailed understanding is required of the various dissipative processes involved. This also will be a topic for future study.

REFERENCES

1. Bikerman, J. J., "Foams." Springer, New York, 1973.
2. Lissant, K. J., *J. Colloid Interface Sci.* **22,** 462 (1966).
3. Nixon, J., and Beerbower, A., *Amer. Chem. Soc. Div. Petrol. Chem. Prepr.* **14,** 49 (1969).
4. Mannheimer, R. J., *J. Colloid Interface Sci.* **40,** 370 (1972).
5. Princen, H. M., *J. Colloid Interface Sci.* **71,** 55 (1979).
6. Princen, H. M., Aronson, M. P., and Moser, J. C., *J. Colloid Interface Sci.* **75,** 246 (1980).

7. Aronson, M. P., and Princen, H. M., *Nature (London)* **286,** 370 (1980).
8. Aronson, M. P., and Princen, H. M., *Colloids Surf.* **4,** 173 (1982).
9. Bikerman, J. J., "Foams," p. 61. Springer, New York, 1973.
10. Hansen, R. S., and Derderian, E. J., *in* "Foams" (R. J. Akers, Ed.), p. 7. Academic Press, London, 1976.
11. Schwarz, H. W., *Rec. Trav. Chim.* **84,** 771 (1964).
12. Neumann, A. W., *Forschungen Fortschritte* **40,** 229 (1966).
13. Lamarle, E., *Mém. Acad. Roy. Sci. Belg.* **35,** (1885); **36** (1867). Cited in Ref. (12).
14. Plateau, J., *Mém. Acad. Roy. Sci. Belg., 5th Ser.* **33** (1861). Cited in Ref. (9).
15. Padday, J. F., Pitt, A. R., and Pashley, R. M., *J. Chem. Soc. Faraday Trans. I* **71,** 1919 (1975).
16. Huh, C., and Mason, S. G., *Canad. J. Chem.* **54,** 969 (1976).
17. Boucher, E. A., and Kent, H. J., *J. Chem. Soc. Faraday Trans. I* **74,** 846 (1978).
18. Boucher, E. A., and Kent, H. J., *Proc. R. Soc. Lond. A* **356,** 61 (1977).
19. Boucher, E. A., *Proc. R. Soc. Lond. A* **358,** 519 (1978).
20. Prins, A., *in* "Foams" (R. J. Akers, Ed.), p. 51. Academic Press, London, 1976.